Annals of Nuclear Medicine Vol. 21, No. 1, 47–55, 2007

Comparison of dynamic FDG-microPET study in a rabbit turpentine-induced inflammatory model and in a rabbit VX2 tumor model

Yoshimasa HAMAZAWA,* Koichi KOYAMA,* Terue OKAMURA,** Yasuhiro WADA,***,**** Tomoko WAKASA,***** Tomohisa OKUMA,* Yasuyoshi WATANABE***,**** and Yuichi INOUE*

*Department of Radiology, Osaka City University Graduate School of Medicine
**PET Center, Saiseikai Nakatsu Hospital, Osaka
***Department of Physiology, Osaka City University Graduate School of Medicine
****RIKEN
*****Department of Pathology, Osaka City University Hospital

Purpose: We investigated the optimum time for the differentiation tumor from inflammation using dynamic FDG-microPET scans obtained by a MicroPET P4 scanner in animal models. ***Materials and Methods:*** Forty-six rabbits with 92 inflammatory lesions that were induced 2, 5, 7, 14, 30 and 60 days after 0.2 m*l* (Group 1) or 1.0 m*l* (Group 2) of turpentine oil injection were used as inflammatory models. Five rabbits with 10 VX2 tumors were used as the tumor model. Helical CT scans were performed before the PET studies. In the PET study, after 4 hours fasting, and following transmission scans and dynamic emission data acquisitions were performed until 2 hours after intravenous FDG injection. Images were reconstructed every 10 minutes using a filtered-back projection method. PET images were analyzed visually referring to CT images. For quantitative analysis, the inflammation-to-muscle (I/M) ratio and tumor-to-muscle (T/M) ratio were calculated after regions of interest were set in tumors and muscles referring to CT images and the time-I/M ratio and time-T/M ratio curves (TRCs) were prepared to show the change over time in these ratios. The histological appearance of both inflammatory lesions and tumor lesions were examined and compared with the CT and FDG-microPET images. ***Results:*** In visual and quantitative analysis, All the I/M ratios and the T/M ratios increased over time except that Day 60 of Group 1 showed an almost flat curve. The TRC of the T/M ratio showed a linear increasing curve over time, while that of the I/M ratios showed a parabolic increasing over time at the most. FDG uptake in the inflammatory lesions reflected the histological findings. For differentiating tumors from inflammatory lesions with the early image acquired at 40 min for dual-time imaging, the delayed image must be acquired 30 min after the early image, while imaging at 90 min or later after intravenous FDG injection was necessary in single-time-point imaging. ***Conclusion:*** Our results suggest the possibility of shortening the overall testing time in clinical practice by adopting dual-time-point imaging rather than single-time-point imaging.

Key words: tumor, inflammation, FDG, microPET, dual-time point imaging

INTRODUCTION

THE UTILITY of ^{18}F-fluorodeoxyglucose (FDG)-PET in the evaluation of patients with cancer has been established clinically in recent years. FDG-PET is reported to be useful for differentiating malignant tumors from benign, staging malignant tumors, diagnosing recurrent tumor, evaluating the therapeutic effect, and prognosis.[1–3] However, FDG-PET has limitations for differentiation

Received September 29, 2006, revision accepted November 2, 2006.

For reprint contact: Yoshimasa Hamazawa, Department of Radiology , Osaka City University, Graduate School of Medicine, Medical School, 1–4–3 Asahi-machi, Abeno-ku, Osaka 545–8585, JAPAN.

E-mail: yoshi-h@med.osaka-cu.ac.jp

between inflammatory lesions and malignant tumors, because FDG uptake in inflammatory lesions is often shown as high as in malignant tumors.[4,5] For improving the diagnostic impact of FDG-PET, the dual-time-point imaging by which delayed images are acquired at 2 hours or more after the intravenous injection of FDG in addition to the usual 1 hour images is reported to be useful in various tumors, such as head and neck tumors, pancreatic tumors, lung tumors, and mediastinal metastatic tumors.[6–10] Additional delayed imaging was reported to be acquired at 2 hours, 3 hours, etc., and mostly acquired at 2 hours, but there is no clear consensus on the optimum time for delayed imaging. Nakamoto et al. reported that the diagnostic value of the delayed images acquired at 3 hours showed no difference compared to those acquired at 2 hours on pancreatic tumors.[10] This result suggests that there was no need to wait more than 2 hours after the intravenous injection of FDG for acquiring delayed images. The patient is required to fast for a longer period for additional delayed imaging, which could be stressful. Acquiring the delayed image earlier would reduce this stress on patients.

There have been some animal studies on changes in FDG uptake by inflammatory and tumor lesions over time, but most of these involved the measurement of activity after the removal of inflammatory or tumor tissues[11] or by means of clinical PET scanner.[12] Recently, the microPET scanner has been developed as a high-resolution PET scanner for use with animals and has been used to investigate the FDG uptake of tumors or inflammation in animals.[13–15] As for the animal studies using microPET on inflammatory and tumor lesions, some studies have reported changes in FDG uptake over time in tumor lesions only[16] and FDG uptake at specific time points in inflammation lesions[17] or comparison between inflammatory and tumor lesions.[18] To our knowledge, no comparative study of FDG uptake in tumors and inflammation lesions has been conducted using dynamic FDG-microPET.

We therefore conducted an animal study using an inflammation model and a tumor model, acquired continuous FDG-PET images with a microPET for up to 2 hours, and studied the images to determine the optimum time for acquiring additional delayed images for differentiating inflammatory lesions from malignant lesions effectively.

MATERIALS AND METHODS

Animal

Inflammation models

Forty-six Japanese white rabbits with 92 inflammatory lesions were used in this study. Inflammatory lesions were made by turpentine oil (KANTO CHEMICAL Co., Inc., Tokyo, Japan) injection into bilateral paravertebral muscles after sedation by an intramuscular injection of ketamine (80 mg) and xylazine (8 mg).

Calculations of turpentine oil requirement per unit body weight based on rat studies suggest that 3 m*l* is necessary for a 2 kg rabbit.[19] However, when 3 m*l* of turpentine oil was used to induce inflammation, it resulted in abscesses elongated along the cephalocaudal direction, with a lot of seepage of oil into the subcutaneous tissue, making it impossible to create stable inflammatory lesions. Nonetheless, stable inflammatory lesions could be created with 1 m*l* and 0.2 m*l* turpentine oil, and therefore, inflammatory lesions were created with 0.2 m*l* (Group 1) and 1.0 m*l* (Group 2) of turpentine oil in this study. In both groups, scans were performed on 4 rabbits (8 lesions) each at 2, 5, 7 and 14 days, and on 3 rabbits (6 lesions) each at 30 and 60 days after the turpentine oil injection. These rabbits were sacrificed after the FDG-PET scans and the relation between images and tissue histological findings was investigated. Changes over days were studied up to 60 days in the same 2 animals (4 lesions) from each group, which were designated as Group 1f and Group 2f. One rabbit of Group 1 at 2 days showed very high uptake in the urinary bladder, which caused a strong artifact effect and quantitative evaluation was impossible, so that this rabbit was excluded from this study.

Tumor models

Five Japanese white rabbits with 10 tumors were used, which had been transplanted VX2 tumors in the bilateral calf muscles 2 weeks earlier. VX2 carcinoma was obtained from Kyowa Hakko Industry (Tsukuba, Japan) and was maintained as a tumor line in allogeneic rabbits in our laboratory. After sedation by an intramuscular injection of ketamine (80 mg) and xylazine (8 mg), the VX2 carcinoma previously implanted in the thighs of allogeneic rabbits was surgically removed. The tumor was then incised with scissors, subjected to forceful pipetting, and filtered through a stainless steel mesh to obtain a suspension of single tumor cells. The tumor suspension (0.5 m*l*, approximately 1×10^7 tumor cells) was injected into bilateral calf muscles.

Image acquisition

FDG-microPET imaging was performed immediately after CT scans in all cases. For the inflammatory lesions of Group 1f and Group 2f, CT scanning was performed only before the initial FDG-microPET imaging, and only FDG-microPET imaging was performed in the subsequent follow-up because we could not take the experimental animals out of our isotope research facility due to certain regulations.

CT system and data acquisition

The single-helical CT (Pro Speed AI, General Electric Medical Systems, Milwaukee, WI, USA) was used in this study. The images were acquired with technical parameters of 120 kV, 100 mAs, 2.0 mm slice thickness,

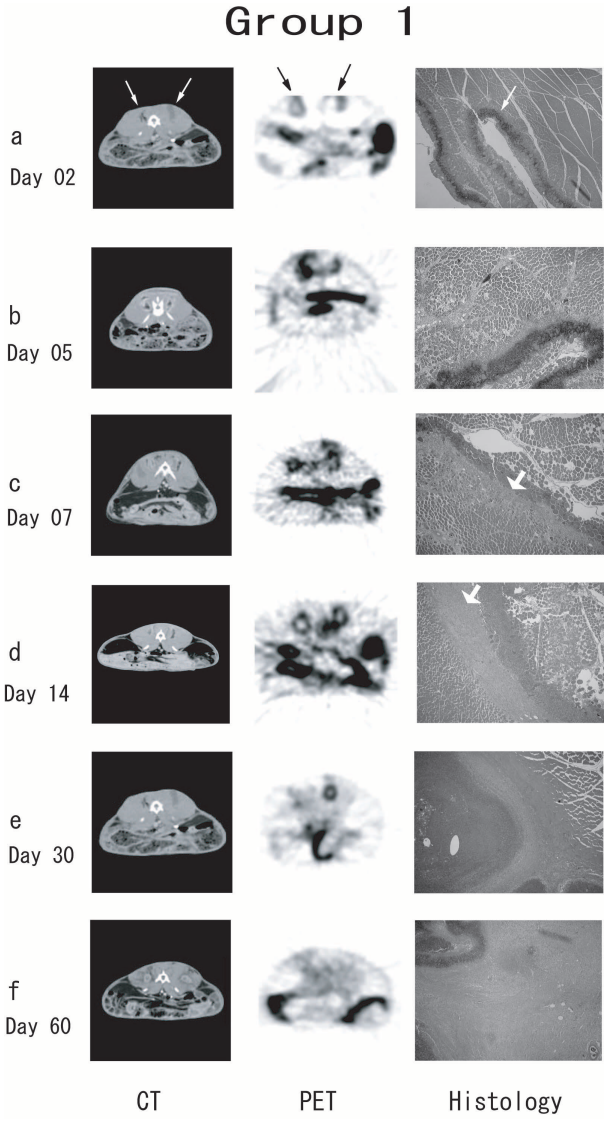

Fig. 1 The enhanced CT images (*left*), the FDG-microPET images (*middle*) and the photomicrograph stained by H-E (*right*) of inflammatory lesions induced in the bilateral paravertebral muscles on 2 days (a), 5 days (b), 7 days (c), 14 days (d), 30 days (e) and 60 days (f) after 0.2 m*l* turpentine oil injection. The CT images and the FDG-microPET images were on prone position. The enhanced CT images demonstrated the ring-like enhancement around the central low density area considered as oil or necrosis, and this enhancement were highly visible on day 5 to day 30 (*arrow*). The FDG-microPET images showed the high uptakes in the bilateral paravertebral muscles (*arrow*) corresponding to the enhanced lesions in CT images. Photomicrographs were H-E stained and showed as ×40. Photomicrographs demonstrated histiocytes layer (*narrow arrow*) and granulation layer around oil pooling (*wide arrow*).

and reconstruction interval of 2.0 mm. Non-contrast and contrast CT scans were performed. Two milliliters per body weight (kg) of iodinated contrast medium was administratered as a bolus via an ear vein by hand injection, and the enhanced CT scanning was started at 80 seconds after the intravenous injection.

MicroPET system and data acquisition

The MicroPET P4 system (Concorde Microsystems Inc., Knoxville, TN, USA) was used in this study. The system is composed of 168 detector modules, each with an 8 × 8 array of 2.2 × 2.2 × 10 mm^3 lutetium oxyorthosilicate (LSO) crystals, arranged as 32 crystal rings 26 cm in diameter. The detector crystals are coupled to Hamamatsu R5900-C8 position-sensitive photo-multiplier tubes (PS-PMT) via 10 cm long optical fiber bundles with a spatial resolution of 1.75 mm full-width of a half maximum (FWHM) at the center of the field of view (FOV). It has a 7.8 cm axial extent, a 19 cm diameter transaxial FOV and a 22 cm animal port. The data were stored in the list-mode by a host PC running Windows XP.

The animals with inflammatory lesions or tumor lesions were anesthetized with intramuscular administration of ketamine (80 mg) and xylazine (8 mg) after a 4-hour fast. After securing the rabbits with a fixative material, transmission scans were performed for 15 min with an 18 MBq $^{68}Ge/^{68}Ga$ point source to obtain attenuation correction data. Then, 55–111 MBq of ^{18}F-FDG was administered intravenously at a maximum volume of 2.0 m*l* via an ear vein. After the intravenous FDG injection, the emission data were acquired dynamically for 2 hours with an energy window of 350–650 keV and a coincidence timing window of 6 ns. All emission scans were corrected for random coincidences and normalized for detector efficiencies. The normalized data were collected by the $^{68}Ge/^{68}Ga$ external point source. Images were reconstructed every 10 minutes by a filtered back-projection (FBP) algorithm with attenuation correction. Images were smoothed by using a Gaussian kernel with an FWHM of 1.97 mm in the transverse direction.

Image Analysis

Visual Interpretation

After comparing the FDG-microPET image with the CT image, we visually evaluated FDG uptake in the inflammatory lesions and tumor lesions.

Quantitative Interpretation

Regions of interest (ROIs) of suitable size were set as 3 polygonal ROIs in inflammatory lesions, tumor lesions, and muscle tissue for measuring counts and these means were calculated. For the inflammatory lesions and tumor lesions the ROIs were selected from the areas of highest FDG uptake in them, whereas the muscle ROIs were selected at gluteus muscles not apparently affected by the uptake in inflammatory lesions or tumor lesions. The inflammation-to-muscle (I/M) ratio and tumor-to-muscle (T/M) ratio were calculated from these means. The time-I/M ratio and time-T/M ratio curves (TRCs) were prepared to see the change over time in these ratios. The

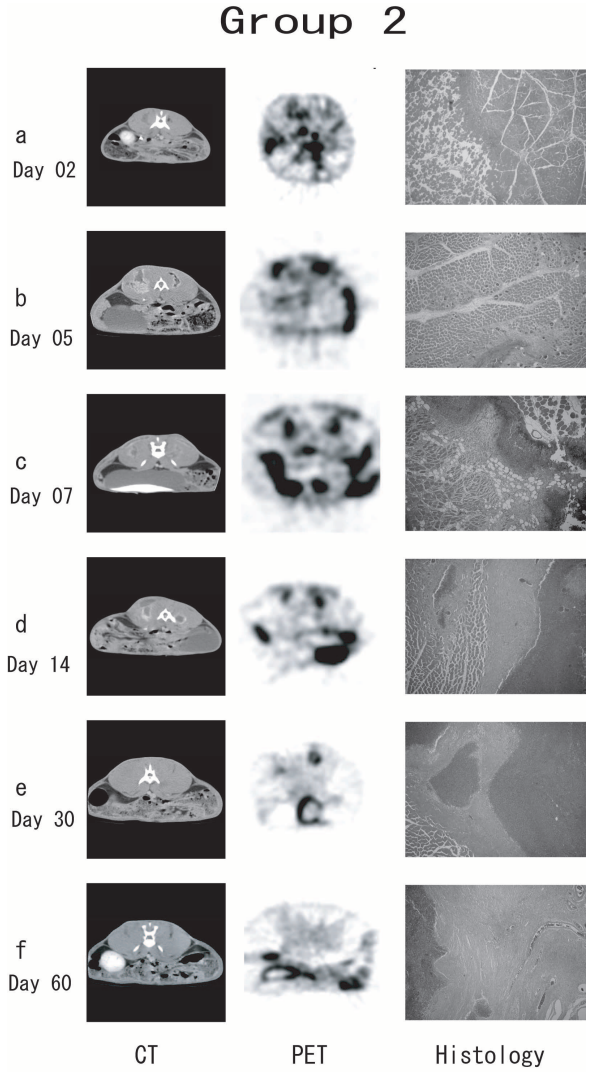

Fig. 2 The enhanced CT images (*left*), the FDG-microPET images (*middle*) and the photomicrograph stained by H-E (*right*) of inflammatory lesions induced in the bilateral paravertebral muscles on 2 days (a), 5 days (b), 7 days (c), 14 days (d), 30 days (e) and 60 days (f) after 1.0 m*l* turpentine oil injection. The enhanced CT images demonstrated the ring-like enhancement around the central low density area considered as oil or necrosis. The FDG-microPET images showed the high uptakes in the bilateral paravertebral muscles corresponding to the enhanced lesions in CT images. Photomicrographs were H-E stained and showed as ×40. Photomicrographs demonstrated histiocytes layer and granulation layer around oil pooling.

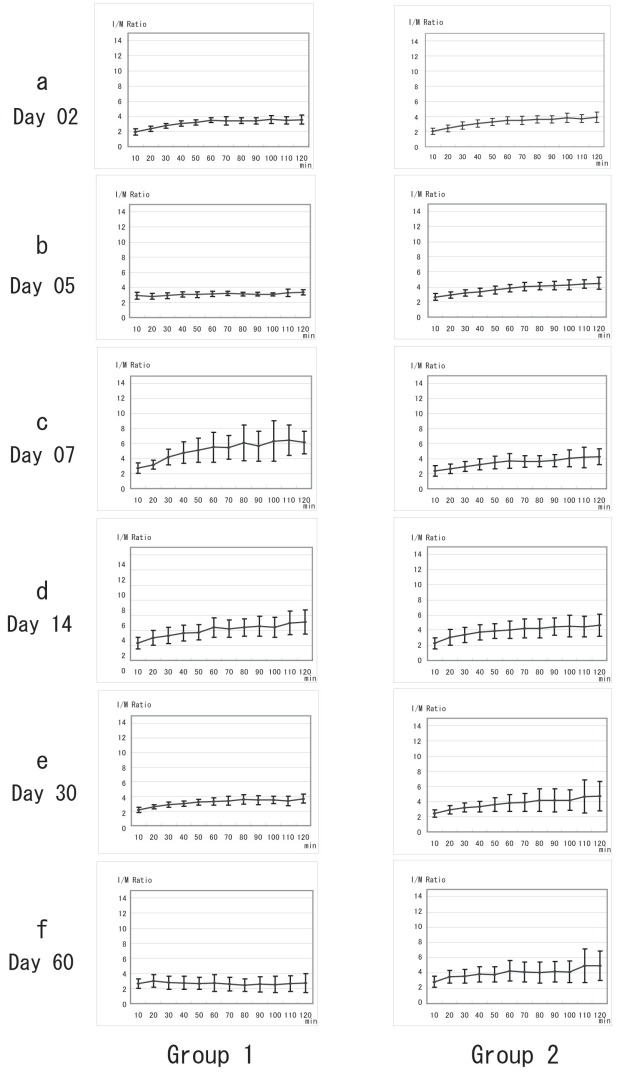

Fig. 3 The TRCs of the I/M ratio in Group 1 (*left side*) and Group 2 (*right side*) on 2 days (a), 5 days (b), 7 days (c), 14 days (d), 30 days (e) and 60 days (f) after turpentine oil injection.

non-parametric Wilcoxon rank sum test was used for testing statistical significance, taking $p < 0.05$ as significant.

Histological findings

After acquiring FDG-microPET imaging, the animals were sacrificed promptly and their tissues were removed. Their tissue sections were prepared after fixation in formalin, and then they were H-E stained. The histological appearance of both inflammatory lesions at different time points and tumor lesions were examined and compared with the CT and FDG-microPET images.

RESULTS

Inflammatory lesions

CT image

CT, FDG-microPET and histological images of each time point in Group 1 and Group 2 are summarized in Figure 1 and Figure 2, respectively. The size in the anterioposterior direction ranged from 2 cm to 5 cm in both groups. The site where the turpentine oil was injected into the paravertebral muscle showed a low density on plain CT images, and a ring like enhancement was seen around the low-density area on the enhanced CT images. There were no

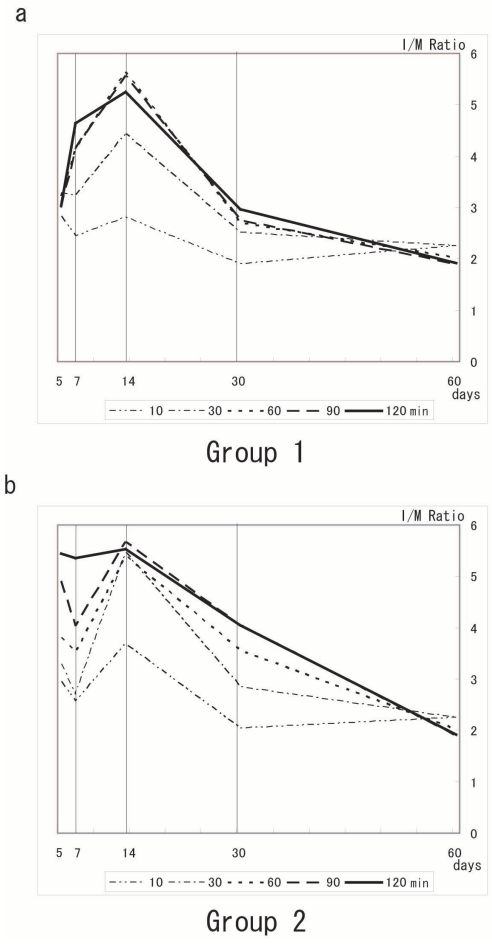

Fig. 4 The change of the I/M ratios obtained 10, 30, 60, 90 and 120 min after intravenous FDG injection from day 5 to day 60 after oil injection in Group 1f (a) and Group 2f (b). The I/M ratio of each obtained minutes showed highest on day 14 in both groups.

major changes in the shape of the image from Day 2 to Day 60. Group 2 had a larger and more spreading low-density area in the cephalocaudal direction along the muscle fibers than Group 1.

FDG-microPET image

Visual evaluation of Group 1 yielded the following findings (Fig. 1). FDG uptake was relatively low on Day 2. On Day 5, The FDG uptake became higher and showed an increasing trend over time. The uptake was higher on Day 7 and Day 14 than on Day 5. On Day 7 and 14, the uptakes showed an increasing trend up to 2 hours, but these had low uptake areas in the center. The uptake was low on Day 30 and Day 60 compared to Day 7 or 14, and especially on Day 60 the uptake was low and showed little change over time. In Group 2, the results of each time point were similar to those of Group 1 (Fig. 2), but on Day 60 there was higher FDG uptake than in Group 1 and it showed a mild increasing trend up to 2 hours. Group 1f and Group 2f also showed similar uptakes as mentioned above for Group 1 and Group 2 respectively.

For quantitative evaluation, the I/M ratio of Group 1 and the T/M ratio are shown in Table 1. The I/M ratio of Group 2 and the T/M ratio are shown in Table 2. The TRCs of the I/M ratio at each time point for both amounts of oil are shown in Figure 3. The TRCs of the I/M ratio in Group 1 and Group 2 showed parabolic increasing curves over time except that on Day 60 of Group 1, which showed no change over time. In Group 1f and Group 2f, the TRCs of the I/M ratio of each time point showed parabolic increasing curves similar to those of Group 1 and Group 2, respectively. The I/M ratios of both groups remained high up to 2 hours on Day 14 compared to the other days and showed low ratios on Days 30 and 60 (Fig. 4).

Histological findings

Group 1 and Group 2 gave similar histological results (Figs. 1, 2). On Day 2, histiocyte invasion was seen around the injected oil. On Day 5, the histiocyte layer had become thicker and showed signs of acute inflammation, a central necrotic area with oil pooling was seen, and fibroblasts were observed around the histiocytes. From Day 7, a granulation layer of proliferating fibroblasts suggestive of chronic inflammation was observed. On Day 14, the granulation layer had thickened further and residual oil and necrosis were seen in the center. On Days 30 and 60, the granulation layer had enlarged almost encircling the central necrotic area, neovascularization was observed around the granulation layer, and the layer associated with acute inflammation had shrunk.

Tumor lesions

CT image

CT, FDG-microPET and histological images of each time point are summarized in Figure 5. Tumor lesions were found as masses on both calf muscles. The size of tumors ranged from 2 cm to 5 cm in diameter. The low-density areas in the center of the masses were seen on plain CT images, and a ring like enhancement was seen in the peripheral lesions of the masses on enhanced CT images. The size of peripheral ring enhancement showed almost the same thickness, while the central low density area showed differences in size between tumors.

FDG-microPET image

Visual evaluation revealed a ring-shaped pattern of high FDG uptake and increasing uptake over time. Quantitative evaluation showed that T/M ratio increased over time, the TRC of the T/M ratio showed a linear increasing curve (Fig. 5).

Histological findings

The mass had peripheral viable tumor tissues and central necrotic tissues. The outside region of the viable tumor tissues had mild infiltration of inflammatory cells.

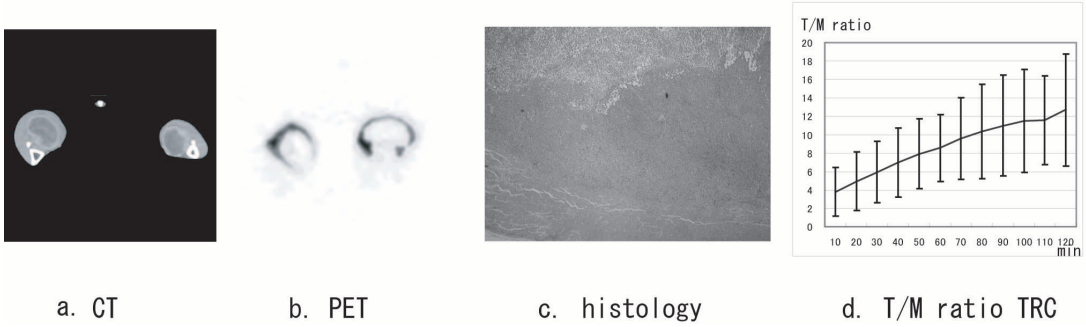

Fig. 5 The enhanced CT images (a), the FDG-microPET images (b), the photomicrograph stained by H-E (c) and the TRC of T/M ratio (d) of a rabbit with VX2 tumor in the bilateral thighs.

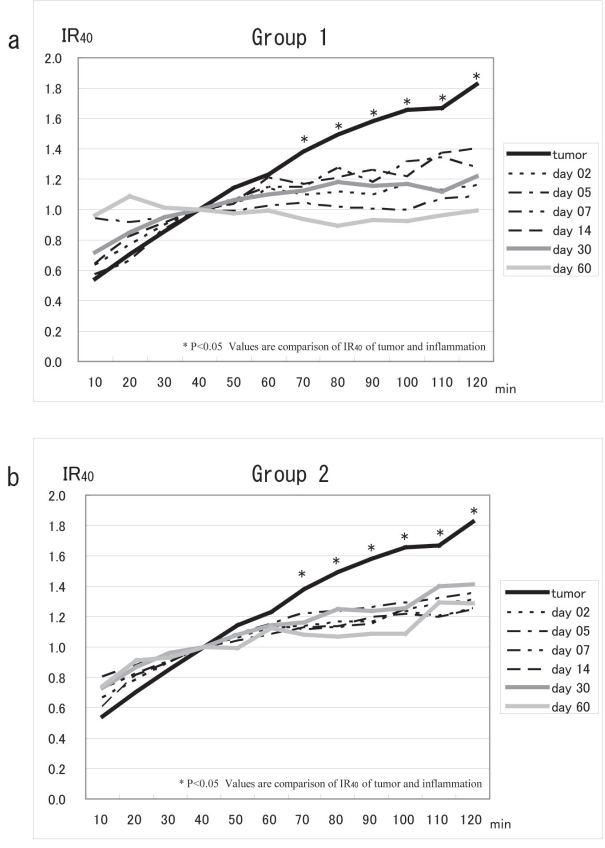

Fig. 6 The time-ratio using the I/M ratio or T/M ratio at 40 min after intravenous FDG injection (TR_{40}). The TR_{40} of the I/M ratio on all days increased over time except the RI of Group 1 on Day 60 showing the horizontal curve. The TR_{40} of the T/M ratio showed a linear increasing curve. There was a significant difference after 70 min between the TR_{40} of tumor lesions and that of inflammatory lesions of both groups on all days.

Statistical analysis

Regarding the I/M ratios of Group 1 (Table 1), the I/M ratio on Day 7 showed a significant difference from 90 min after intravenous FDG injection with the T/M ratio. The I/M ratios on Days 2 and 60 showed a significant difference from 30 min with the T/M ratio. The I/M ratio on Days 2, 5, 14, 30 and 60 showed a significant difference from 40 min with the T/M ratio. Regarding the I/M ratios of Group 2 (Table 2), the I/M ratios on Days 2, 5, 7 and 60 showed a significant difference from 40 min after intravenous FDG injection with the T/M ratio. The I/M ratio on Days 14 and 30 showed a significant difference from 50 min with the T/M ratio.

As described above, most of the I/M ratios showed a significant difference from 40 min with the T/M ratio, and therefore, the increasing rate using the I/M ratio or T/M ratio at 40 min after intravenous FDG injection (IR_{40}) was defined as below; I/M ratio or T/M ratio divided by the I/M ratio or the T/M ratio at 40 min after intravenous FDG injection. The IR_{40} of the I/M ratios of both groups and that of the T/M ratio area are shown in Figure 6. The IR_{40} of the I/M ratio on all days increased over time except that the RI of Group 1 on Day 60 showed a horizontal curve. The IR_{40} of the T/M ratio showed a linear increasing curve. There was a significant difference between the tumor lesions and the inflammatory lesions of both groups on all days since 70 min or more after intravenous injection.

DISCUSSION

It is often difficult to differentiate tumors from inflammatory lesions using FDG-PET, because both show high FDG uptake. Additional delayed images are reported to have the capability to improve the diagnostic impact. Although there is no clear consensus on the appropriate time to acquire the delayed images, it is desirable to acquire them as early as possible, considering the stress caused to the patient because of the long fasting period requirement. MicroPET scanner also gives a higher resolution than clinical PET scanner. We therefore performed continuous FDG-microPET imaging for up to 2 hours using a microPET with rabbits having inflammatory or tumor lesions to decide the optimum time point for acquiring the additional delayed image.

Even in the 0.2 m*l* group on Day 7, which showed the highest uptake by inflammatory lesions, there were significant differences between I/M and T/M from 90 min

Table 1 I/M ratio of Group 1 and T/M ratio

time (min)	2 days after injection[#]	5 days after injection[#]	7 days after injection[#]	14 days after injection[#]	30 days after injection[#]	60 days after injection[#]	Tumor[#]
10	1.95 ± 0.41	2.90 ± 0.48	2.74 ± 0.69	2.33 ± 0.76	2.16 ± 0.34	2.65 ± 0.65	3.79 ± 2.65
20	2.36 ± 0.35*	2.81 ± 0.39	3.17 ± 0.58	2.98 ± 0.97	2.57 ± 0.30	2.99 ± 0.84	4.91 ± 3.18
30	2.77 ± 0.30*	2.92 ± 0.37	4.20 ± 1.07	3.29 ± 1.08	2.88 ± 0.35	2.79 ± 0.87*	5.93 ± 3.34
40	3.07 ± 0.36*	3.06 ± 0.33*	4.79 ± 1.46	3.60 ± 1.05*	3.02 ± 0.35*	2.75 ± 0.86*	6.94 ± 3.76
50	3.20 ± 0.37*	3.05 ± 0.38*	5.13 ± 1.63	3.73 ± 1.01*	3.22 ± 0.39*	2.68 ± 0.80*	7.93 ± 3.76
60	3.50 ± 0.32*	3.14 ± 0.32*	5.50 ± 1.98	4.36 ± 1.31*	3.31 ± 0.50*	2.73 ± 1.10*	8.56 ± 3.66
70	3.39 ± 0.55*	3.20 ± 0.30*	5.50 ± 1.61	4.20 ± 1.14*	3.40 ± 0.58*	2.58 ± 0.92*	9.58 ± 4.41
80	3.44 ± 0.40*	3.11 ± 0.26*	6.10 ± 2.36	4.36 ± 1.18*	3.57 ± 0.65*	2.45 ± 0.82*	10.36 ± 5.14
90	3.39 ± 0.43*	3.08 ± 0.25*	5.66 ± 1.99*	4.56 ± 1.33*	3.48 ± 0.62*	2.56 ± 1.02*	10.97 ± 5.48
100	3.59 ± 0.54*	3.07 ± 0.20*	6.33 ± 2.68*	4.39 ± 1.32*	3.53 ± 0.50*	2.54 ± 1.09*	11.50 ± 5.59
110	3.48 ± 0.49*	3.30 ± 0.49*	6.44 ± 2.02*	4.96 ± 1.57*	3.38 ± 0.64*	2.65 ± 1.07*	11.59 ± 4.82
120	3.58 ± 0.62*	3.33 ± 0.34*	6.15 ± 1.51*	5.08 ± 1.61*	3.68 ± 0.59*	2.72 ± 1.27*	12.69 ± 6.12

[#]Mean ± S.D. *$p < 0.05$ Values are comparison of tumor/muscle ratio

Table 2 I/M ratio of Group 2 and T/M ratio

time (min)	2 days after injection[#]	5 days after injection[#]	7 days after injection[#]	14 days after injection[#]	30 days after injection[#]	60 days after injection[#]	Tumor[#]
10	2.07 ± 0.40	2.67 ± 0.45	2.37 ± 0.67	2.26 ± 0.72	2.44 ± 0.48	2.86 ± 0.73	3.79 ± 2.65
20	2.43 ± 0.43	2.91 ± 0.43	2.66 ± 0.63*	3.05 ± 1.02	2.90 ± 0.56	3.51 ± 0.83*	4.91 ± 3.18
30	2.80 ± 0.45	3.21 ± 0.44*	2.94 ± 0.67	3.39 ± 1.00	3.21 ± 0.60	3.59 ± 0.87*	5.93 ± 3.34
40	3.09 ± 0.47*	3.31 ± 0.55*	3.23 ± 0.74*	3.73 ± 1.01	3.34 ± 0.70	3.85 ± 0.99*	6.94 ± 3.76
50	3.29 ± 0.48*	3.61 ± 0.54*	3.51 ± 0.84*	3.88 ± 1.00*	3.61 ± 0.88*	3.84 ± 0.99*	7.93 ± 3.76
60	3.50 ± 0.48*	3.84 ± 0.48*	3.70 ± 0.96*	4.06 ± 1.14*	3.82 ± 1.09*	4.32 ± 1.35*	8.56 ± 3.66
70	3.52 ± 0.55*	4.05 ± 0.56*	3.63 ± 0.76*	4.22 ± 1.27*	3.89 ± 1.18*	4.17 ± 1.32*	9.58 ± 4.41
80	3.61 ± 0.48*	4.11 ± 0.51*	3.66 ± 0.76*	4.25 ± 1.26*	4.18 ± 1.48*	4.11 ± 1.38*	10.36 ± 5.14
90	3.61 ± 0.47*	4.19 ± 0.57*	3.74 ± 0.82*	4.47 ± 1.15*	4.14 ± 1.52*	4.18 ± 1.35*	10.97 ± 5.48
100	3.83 ± 0.62*	4.29 ± 0.69*	4.05 ± 1.13*	4.54 ± 1.42*	4.20 ± 1.34*	4.18 ± 1.40*	11.50 ± 5.59
110	3.72 ± 0.53*	4.39 ± 0.54*	4.16 ± 1.37*	4.48 ± 1.35*	4.68 ± 2.20*	4.97 ± 2.22*	11.59 ± 4.82
120	3.89 ± 0.70*	4.50 ± 0.78*	4.25 ± 1.04*	4.67 ± 1.47*	4.72 ± 1.97*	4.96 ± 1.94*	12.69 ± 6.12

[#]Mean ± S.D. *$p < 0.05$ Values are comparison of tumor/muscle ratio

onwards. I/M ratios on many other days were significantly different from T/M as early as 40 min.

If inflammatory and tumor lesions are to be differentiated at one time point only, the tumor can be differentiated from inflammation with an image acquired at 90 min or later.

As FDG uptake in tumor lesions was significantly different from those in inflammatory lesions after 40 min on most of the observations days, the optimum imaging time for additional delayed images was investigated using retention indices as shown in the results when the early image was acquired at 40 min. For the experimental models used in this study, the delayed image could be acquired at 70 min, the time point at which significant differences in the retention index started showing up. Thus, it became clear that a time lag of 30 min was required after the early imaging.

The procedure for creating inflammatory lesions with turpentine oil is simple and easy, and therefore it is an effective method. Inflammatory lesions as one of the observation targets in this study were induced using 0.2 m*l* and 1 m*l* of turpentine oil, and both amounts induced stable inflammatory lesions. In the lesions created with 1 m*l*, the inflammation persisted for a long time, and did not enter the healing phase up to Day 60. Meanwhile, in the lesions induced with 0.2 m*l* oil, the inflammation subsided by Day 60 to an extent where abnormal FDG uptake was not observed. This means that we can make observations at the acute, chronic and healing phases of the inflammation.

FDG uptake in the inflammatory lesions was mildly elevated on Day 2. The uptake increased over time from Day 2 up to Day 14, but it became less by Day 30 and Day 60. Zhao et al. reported that the FDG uptake in turpentine oil-induced inflammation declined within 2 weeks as the inflammation cleared.[20] These findings differ from our results, probably because they used a different absolute amount of turpentine oil, and the experimental animals were rats.

In our study, histological examination of the tissue showed histiocyte infiltration from Day 2 as a sign of acute inflammation. The histiocyte infiltration peaked on

Day 7 and decreased by Day 14. Fibroblasts appeared on Day 5, and their number peaked on Day 14. The changes in FDG uptake with the passage of days seemed to reflect FDG uptake in these tissues. Kaim et al. reported that FDG uptake was seen in histiocytes and fibroblasts.[21] Our results support their findings. Proliferation of collagen fibers was seen on Day 30 and Day 60 in the parts where the fibroblasts were seen earlier, and this was the likely cause of the observed lack of FDG uptake.

From Day 2 to Day 14, the 0.2 m*l* turpentine oil group (Group 1) and the 1.0 m*l* group (Group 2) did not differ in FDG uptake or histological appearance. However, on Day 30 and Day 60 inflammatory lesions of Group 2 showed higher uptake than those of Group 1. This difference may be due to the difference in the amount of oil. In other words, in the inflammatory lesions induced with large amounts of oil, it took longer for the oil absorption and the acute inflammation zone to shrink and undergo fibrosis in the healing process.

The tumor lesions showed no FDG uptake in the central necrotic area, but the surrounding area of viable tumor cells showed increased FDG uptake over time. Chang et al. investigated lung carcinoma-bearing mice with microPET and reported that the FDG uptake reached a plateau at 60 min and after that uptake became lower up to 120 min.[1]

Kok et al. investigated FDG uptake in tumors and inflammation using LS174T tumor-bearing rats and rats with *Escherichia coli* inducing infectious inflammation until 4 hours after FDG intravenous injection.[22] They also reported that the increase of the FDG uptake during the first 1 hour was significantly higher and faster in the abscess than in the tumor, but FDG uptake of both remained stable during the next 3 hours. These findings differ from our results, probably because they used a different type of tumor.

There may be some limitations in clinical application using the results of this study.

One of the limitations is that turpentine oil-induced inflammation is a chemical inflammation. Regarding the chemical nature of the turpentine oil-induced inflammation, the results may be clinically applicable in certain cases because sometimes there are non-bacterial chemical inflammations such as very acute pancreatitis. Also, Zhao et al. reported that there was no significant difference in FDG uptake between Streptococcus-induced and turpentine oil-induced inflammation.[23] Okuma et al. reported that ring-shaped FDG uptakes were seen after radiofrequency ablation of normal lungs coinciding with inflammation and the highest FDG uptakes were seen after 7 to 14 days after radiofrequency ablation.[24] Their results had the same duration of inflammation as our results. Studying FDG uptake in turpentine oil-induced inflammation may not yield the same results as with other kinds of inflammatory lesions, but it is meaningful as a method of studying inflammatory lesions.

Another limitation is that the test animals were rabbits, which have very high intestinal uptake. We cannot rely on the SUV values for quantitative evaluation, because rabbits show high levels of physiological uptake in the intestine as pointed out by Ishii et al.[25,26] Therefore, we used the same I/M and T/M ratios for evaluation as Ishii et al. used in their study. The T/M ratio showed a linear increase over time, but the increase of the I/M ratio over time was linear on none of the days, and the increase was mild at most.

The limitations also include that the VX2 tumor used to make the tumor lesions is a very malignant tumor. The significant difference observed could be because of the very malignant nature of the VX2 tumor and we cannot extend these results directly to clinical application. It is interesting that the significant difference in uptake between the tumor lesions and inflammatory lesions of all the stages appeared after no less than 90 min in spite of the high malignancy of the tumor.

Using microPET scanner, the changes in FDG uptake in inflammatory lesions over time could be observed in the same animals on different days, although some animals had to be sacrificed at different stages in the present study for correlating the uptake with the histological findings.

CONCLUSION

We investigated the optimum time for acquiring delayed images, by continuous FDG-PET imaging up to 2 hours after intravenous FDG injection, using inflammation and tumor lesions created in rabbits. Imaging at 90 min or later after intravenous FDG injection was necessary for differentiating malignant from benign lesions in single-time-point imaging. With dual-time imaging, it may be necessary to acquire the delayed image 30 min after the early image under the condition that the early image is acquired at 40 min. Thus, the FDG-PET study could be completed earlier with dual-time-point imaging than with single-time-point imaging.

ACKNOWLEDGMENTS

The authors are greatly indebted to Dr. Satoko Kondo, Dr. Kentaro Ishii, and the staff of the Department of Physiology for their help.

REFERENCES

1. Schmidt GP, Haug AR, Schoenberg SO, Reiser MF. Whole-body MRI and PET-CT in the management of cancer patients. *Eur Radiol* 2006; 16: 1216–1225.
2. Macapinlac HA. FDG-PET in head and neck, and thyroid cancer. *Chang Gung Med J* 2005; 28: 284–295.
3. Mody RJ, Pohlen JA, Malde SS, Peter J, Shulkin BL. FDG PET for the study of primary hepatic malignancies in children. *Pediatr Blood Cancer* 2006; 47: 51–55.

4. Rosenbaum SJ, Lind T, Antoch G, Bockisch A. False-Positive FDG PET Uptake—the Role of PET/CT. *Eur Radiol* 2006; 16: 1054–1065.
5. Barrington SF, O'Doherty MJ. Limitations of PET for imaging lymphoma. *Eur J Nucl Med Mol Imaging* 2003; 30 Suppl 1: S117–S127.
6. Kumar R, Loving VA, Chauhan A, Zhuang H, Mitchell S, Alavi A. Potential of dual-time-point imaging to improve breast cancer diagnosis with (^{18})F-FDG PET. *J Nucl Med* 2005; 46: 1819–1824.
7. Shih YM, Lai CS, Chyong HL, Hung HC, Chien ST. Delayed ^{18}F-FDG PET for Detection of Paraaortic Lymph Node Metastases in Cervical Cancer Patients. *J Nucl Med* 2003; 44: 1775–1783.
8. Hustinx R, Smith RJ, Benard F, Rosenthal DI, Machtay M, Alavi A, et al. Dual time point fluorine-18 fluorodeoxyglucose positron emission tomography: a potential method to differentiate malignancy from inflammation and normal tissue in the head and neck. *Eur J Nucl Med* 1999; 26: 1345–1348.
9. Lyshchik A, Higashi T, Nakamoto Y, Fujimoto K, Doi R, Saga T, et al. Dual-phase ^{18}F-fluoro-2-deoxy-D-glucose positron emission tomography as a prognostic parameter in patients with pancreatic cancer. *Eur J Nucl Med Mol Imaging* 2005; 32: 389–397.
10. Nakamoto Y, Higashi T, Sakahara H, Tamaki N, Kogire M, Konishi J, et al. Delayed ^{18}F-fluoro-2-deoxy-D-glucose positron emission tomography scan for differentiation between malignant and benign lesions in the pancreas. *Cancer* 2000; 89: 2547–2554.
11. Sun YL, Jan ML, Kao PF, Fan KH, Hsu HT, Lee TW, et al. Coincidence planar imaging for dynamic [^{18}F]FDG uptake in nude mice with tumors and inflammation: correlated with histopathology and micro-autoradiography. *Kaohsiung J Med Sci* 2005; 21: 258–266.
12. Zhuang H, Pourdehnad M, Lambright ES, Yamamoto AJ, Lanuti M, Alavi A, et al. Dual Time Point ^{18}F-FDG PET Imaging for Differentiating Malignant from Inflammatory Processes. *J Nucl Med* 2001; 42: 1412–1417.
13. Chatziioannou AF, Cherry SR, Shao Y, Silverman RW, Meadors K, Phelps ME, et al. Performance evaluation of microPET: a high-resolution lutetium oxyorthosilicate PET scanner for animal imaging. *J Nucl Med* 1999; 40: 1164–1175.
14. Tai C, Chatziioannou A, Siegel S, Young J, Newport D, Cherry SR, et al. Performance evaluation of the microPET P4: a PET system dedicated to animal imaging. *Phys Med Biol* 2001; 46: 1845–1862.
15. Kondo S, Hosono MN, Wada Y, Ishii K, Matsumura A, Inoue Y, et al. Use of FDG-microPET for detection of small nodules in a rabbit model of pulmonary metastatic cancer. *Ann Nucl Med* 2004; 18: 51–57.
16. Chang CH, Fan KH, Chen TJ, Hsu WC, Jan ML, Lee TW, et al. Dynamic evaluation of ^{18}F-FDG uptake by microPET and whole-body autoradiography in a fibrosarcoma-bearing mouse model. *J Formos Med Assoc* 2004; 103: 876–881.
17. Pellegrino D, Bonab AA, Dragotakes SC, Pitman JT, Mariani G, Carter EA. Inflammation and Infection: Imaging Properties of ^{18}F-FDG-Labeled White Blood Cells Versus ^{18}F-FDG. *J Nucl Med* 2005; 46: 1522–1530.
18. Chang CH, Wang HE, Wu SY, Fan KH, Tsai TH, Fu YK, et al. Comparative evaluation of FET and FDG for differentiating lung carcinoma from inflammation in mice. *Anticancer Res* 2006; 26: 917–925.
19. Yamada S, Kubota K, Kubota R, Ido T, Tamahashi N. High accumulation of fluorine-18-fluorodeoxyglucose in turpentine-induced inflammatory tissue. *J Nucl Med* 1995; 36: 1301–1306.
20. Zhao S, Kuge Y, Tsukamoto E, Mochizuki T, Kato T, Tamaki N. Fluorodeoxyglucose uptake and glucose transporter expression in experimental inflammatory lesions and malignant tumours: effects of insulin and glucose loading. *Nucl Med Commun* 2002; 23: 545–550.
21. Kaim AH, Weber B, Kurrer MO, Gottschalk J, Von Schulthess GK, Buck A. Autoradiographic quantification of ^{18}F-FDG uptake in experimental soft-tissue abscesses in rats. *Radiology* 2002; 223: 446–451.
22. Kok PJ, van Eerd JE, Boerman OC, Corstens FH, Oyen WJ. Biodistribution and imaging of FDG in rats with LS174T carcinoma xenografts and focal *Escherichia coli* infection. *Cancer Biother Radiopharm* 2005; 20: 310–315.
23. Zhao S, Kuge Y, Tsukamoto E, Mochizuki T, Kato T, Tamaki N, et al. Effects of insulin and glucose loading on FDG uptake in experimental malignant tumours and inflammatory lesions. *Eur J Nucl Med* 2001; 28: 730–735.
24. Okuma T, Matsuoka T, Okamura T, Wada Y, Yamamoto A, Inoue Y. ^{18}F-FDG small-animal PET for monitoring the therapeutic effect of CT-guided radiofrequency ablation on implanted VX2 lung tumors in rabbits. *J Nucl Med* 2006; 47: 1351–1358.
25. Tatsumi M, Nakamoto Y, Traughber B, Marshall LT, Geschwind JF, Wahl RL. Initial Experience in Small Animal Tumor Imaging with a Clinical Positron Emission Tomography/Computed Tomography Scanner Using 2-[F-18]Fluoro-2-deoxy-D-glucose. *Cancer Res* 2003; 63: 6252–6257.
26. Ishii K, Hosono MN, Wada Y, Maeda M, Kondo S, Inoue Y, et al. Usefulness of FDG-microPET for early evaluation of therapeutic effects on VX2 rabbit carcinoma. *Ann Nucl Med* 2006; 20: 123–130.